

1 **Large Ozone Intrusions during Sudden Stratospheric Warmings Enhance**
2 **Ozone Radiative Forcing Over South Asia**

3 Shubhajyoti Roy^{1,2}, Satheesh Chandran PR¹, Suvarna Fadnavis^{1*}, Vijay Sagar¹, Michaela I.
4 Hegglin³, Rolf Müller³, Prashant Chavan¹

5 ¹Indian Institute of Tropical Meteorology, Centre for Climate Change Research, India

6 ²Department of Atmospheric and Space Sciences, Savitribai Phule Pune University, Pune, India

7 ³Institute of Energy and Climate Systems: Stratosphere (ICE-4), Forschungszentrum Jülich,
8 Jülich, Germany

9 *Corresponding author email: suvarna@tropmet.res.in

10
11
12
13
14
15
16
17
18

19 **Abstract**

20 Tropospheric ozone pollution in South Asia is mainly blamed on anthropogenic emissions.
21 However, based on ERA5 reanalysis data, this study highlights the contribution of stratospheric
22 ozone intrusions into the Upper Troposphere and Lower Stratosphere (UTLS) associated with
23 Sudden Stratospheric Warming (SSW) events in enhancing upper tropospheric ozone over the
24 South Asian region, We report an enhancement in UTLS ozone by more than 80% for 2018 and
25 over 30% within ± 6 days of the onset during SSW events concurrent with the westerly phase of
26 the QBO (WQBO-SSW) compared to non-SSW years. The equatorward shift (south of 30°N) of
27 the subtropical jet during WQBO-SSW causes deepening of the tropopause and Rossby-wave
28 penetration in the upper troposphere. This results in more Rossby-wave breaking and
29 stratospheric ozone intrusions over the South Asian region. The ozone enhancement during
30 WQBO-SSW events produces an instantaneous radiative forcing at the top of the atmosphere of
31 $0.09 \pm 0.05 \text{ W.m}^{-2}$ due to UTLS ozone changes and $0.17 \pm 0.05 \text{ W.m}^{-2}$ from total-column ozone
32 changes over South Asia. The elevated tropospheric ozone levels resulting from stratospheric
33 intrusions pose a threat to humans and vegetation.

34

35 **Keywords:** Sudden stratospheric warming, stratosphere intrusions, ozone radiative forcing, South
36 Asian region, Rossby wave breaking.

37 **1. Introduction**

38 Tropospheric ozone is a short-lived greenhouse gas that plays a crucial role in
39 atmospheric chemistry and radiative forcing (Wang et al., 2022). It is also a major air pollutant
40 that significantly affects human health (Lim et al., 2012; Fleming et al., 2018), damages

41 vegetation (Fowler et al., 2009; Feng et al., 2021), disrupts ecosystems, and imposes economic
42 costs (Dewan and Lakhani, 2022). In South Asia, a significant amount of tropospheric ozone is a
43 growing concern due to its increased hazardous health effects (Silva et al., 2013; Lin et al.,
44 2018).

45 The contribution from the downward transport of ozone-rich air from the stratosphere is
46 the largest natural source of tropospheric ozone (e.g., Fadnavis et al., 2010; Roy et al., 2020).
47 Studies have reported that stratospheric influence on the tropospheric ozone exceeds 50% in the
48 winter season at the extratropics (Williams et al., 2019). Wang and Fu (2021) estimate that
49 stratosphere-to-troposphere exchange (STE) contributes approximately 347 ± 12 Tg year⁻¹ to the
50 global tropospheric ozone budget based on both observations and reanalysis data. CMIP6 model
51 simulations from 1997 to 2014 indicate that up to 30% of surface ozone in the Northern
52 Hemisphere during winter (DJF) is due to stratospheric ozone intrusions (Li et al., 2024). In the
53 Northwest Pacific, STE increases mid and upper-tropospheric ozone by about 96% in winter and
54 40% in summer between 1990 and 2020 (Ma et al., 2024). Roy et al. (2023) reported an ozone
55 enhancement of ~40 ppb in the upper troposphere over the Indian region caused by stratospheric
56 intrusions associated with tropical cyclones.

57 Sudden stratospheric warming (SSW) events play a key role in atmospheric dynamics
58 and stratospheric ozone intrusions into the troposphere (e.g., Williams et al., 2024). SSWs are
59 one of the most significant large-scale dynamical phenomena in the stratosphere during winter
60 (Butler et al., 2015; de la Cámara et al., 2018; Baldwin et al., 2021). Enhanced planetary wave
61 activity from the troposphere disrupts the stratospheric polar vortex, decelerating or even
62 reversing the stratospheric westerlies, and causing a rapid rise in polar stratospheric temperatures
63 by up to 50 K within just a few days (Baldwin et al., 2021). SSW events are crucial in

64 modulating extreme heat, air pollution, wildfires, wind extremes, storm clusters, tropical
65 cyclones, and sea ice melt in the northern high latitudes (Domeisen and Butler, 2020; Domeisen
66 et al., 2020). The temperature and wind anomalies associated with SSWs propagate downward
67 into the troposphere over timescales ranging from weeks to months, impacting tropospheric
68 weather in the Northern Hemisphere for up to 40 days following the onset of the event (Baldwin
69 and Dunkerton, 2001; Hall et al., 2021). Studies also suggest that SSWs are often followed by an
70 equatorward shift of the tropospheric jet stream and storm tracks, as well as surface pressure
71 anomalies that resemble the negative phase of the Northern Annular Mode (Sigmond et al., 2013;
72 Kidston et al., 2015). Projection studies suggest that SSW events will increase by approximately
73 one event per decade by the end of the 21st century (Charlton-Perez et al., 2008). High
74 greenhouse gas emission scenarios indicate a doubling in SSW frequency (Schimanke et al.,
75 2012). Considering the frequent occurrences and the potential role of SSWs in STE, it is
76 important to investigate SSWs influence on tropospheric ozone enhancements and the associated
77 radiative effects.

78 SSW events have a significant influence on STE and impact the tropospheric ozone
79 budget, particularly in high-latitude regions (Xia et al., 2023; Williams et al., 2024). Based on 11
80 polar-night jet oscillation (PJO) type SSW events from 1980 to 2013 and chemistry-climate
81 model simulations, STE led to an average increase of 5–10% in near-surface ozone over the
82 Arctic (Williams et al., 2024). Xia et al. (2023) reported an even more pronounced increase of
83 76% in Arctic surface ozone due to STE in the 2020/21 SSW event. While most of these studies
84 focus on the polar regions, some have identified SSW-induced ozone variability in the mid-
85 latitudes (Liu et al., 2009; Lu et al., 2022; Williams et al., 2024). For example, Lu et al. (2022)
86 demonstrated that meteorological changes associated with SSWs cause poor air quality in the

87 Beijing-Tianjin-Hebei region. Liu et al. (2009) noted an ozone enhancement of about 186 Tg in
88 the upper troposphere over East Asia during the 2002–2003 SSW, using MOZART-3
89 simulations. However, tropospheric ozone variations during SSW events over South Asia are
90 among the least studied. Additionally, the broader implications of these events on the ozone
91 radiative forcing over this region remain largely underexplored.

92 In this study, we investigate the impact of all the SSW events from 1962 to 2018 on
93 ozone variability in the upper troposphere and lower stratosphere (UTLS: 300-50 hPa) over the
94 South Asian region (20-35°N, 65-90°E) using ERA5 reanalysis data. The composite is obtained
95 by averaging data with the onset day as a central date (details in the ‘Methods’ section). Here, we
96 report a significant ozone enhancement in the UTLS over South Asia, leading to increased ozone
97 radiative forcing. All SSWs were examined during the period from 1962 to 2018. This revealed
98 more equatorward shift of the subtropical jet over South Asia (~23°N) and associated large
99 ozone intrusion in this region during the 2018 SSW relative to other SSW years. This motivated
100 us to report the detailed mechanism of the 2018 SSW as a case study. A recent study by Shi et al.
101 (2023) reports the influence of the 2018 SSW over East Asia, causing anomalous cooling of
102 18°C. However, to our knowledge, UTLS ozone responses over South Asia during this event
103 have received limited attention, which motivates our emphasis on the 2018 case. We further
104 extend the analysis to all SSWs and assess their contribution to upper-tropospheric ozone and
105 regional ozone radiative forcing.

106 The paper is organised as follows. Section 2 describes the ERA5 reanalysis dataset, the
107 computation of ozone radiative forcing using the radiative-kernel method and dynamical changes
108 in PV during the 2018 event. Section 3 presents the (i) UTLS ozone changes during the 2018

109 SSW event over South Asia, (ii) composite analysis of SSWs, and (iii) ozone radiative forcing.
110 Section 4 summarises the main findings.

111 **2. Methods**

112 **2.1 ERA 5 Reanalysis Data**

113 We analysed daily data of ozone, zonal and meridional winds, geopotential height (GPH),
114 and potential vorticity (PV) from the fifth-generation reanalysis dataset (ERA5) provided by the
115 European Centre for Medium-Range Weather Forecasts (ECMWF) (Hersbach et al., 2020). The
116 ERA5 ozone field is generated through assimilation of multiple satellite- and ground-based
117 observations, including TOMS (1978–2006), SBUV v8.6 (1978–present), CCI MIPAS (2005–
118 2012), SCIAMACHY (2002–2012), Aura MLS v4.2 (2004–present), and OMI-DOAS (2004–
119 present) (Hersbach et al., 2020; S-RIP Final Report, 2022). Comparison of ERA5 ozone with
120 observations shows a slight overestimation in the UTLS. For example, over the North India
121 region, ERA5 show an overestimation of ~20 ppb ozone (Fadnavis et al., 2023). The S-RIP
122 (2022) assessment report states overestimation of ~10–40% between 50°N and 50°S. Overall,
123 ERA5 ozone shows lesser biases than other reanalyses (Fadnavis et al., 2023). We analysed
124 ERA5 ozone, geopotential height, winds, and potential vorticity (PV) data for this study. These
125 variables have a horizontal resolution of $0.25^\circ \times 0.25^\circ$ across 37 standard pressure levels (1000
126 to 1 hPa). Composite analysis is conducted for all variables for ± 30 days, centered on the onset
127 of SSW events (30 days before and after the onset), to assess the impact. The SSW onset is
128 identified as the day when the zonal mean westerly winds at 10 hPa and 60°N reverse their
129 direction from westerlies to easterlies (Charlton and Polvani 2007).

130 Daily anomalies in ozone, geopotential height, winds, and PV during the SSW days were
131 calculated by subtracting the corresponding calendar-day climatology, computed from all the

132 non-SSW years. The long-term trend is removed from the daily ERA5 data before computing
133 anomalies. This approach ensures that anomalies reflect deviations from typical background
134 conditions. To determine statistical significance, we used the Monte Carlo bootstrap and the
135 Wilcoxon signed-rank test. For the Monte Carlo, we built a calendar-matched null by resampling
136 days from non-SSW years within the same day-of-year window. We then use a bias-corrected
137 and accelerated (BCa) bootstrap with 20,000 resamples to form 95% confidence intervals. For
138 2018, we checked whether the observed value lay outside the BCa interval of the background
139 ensemble. For the composite, we tested whether the mean anomaly differed from zero. Next, we
140 applied an exact Wilcoxon signed-rank test to the same data. A grid point is called significant
141 only when both tests agree at 95% significance.

142 The onset of 2018 SSW event is identified as the day when the zonal mean westerly
143 winds at 10 hPa and 60°N reverse their direction from westerlies to easterlies (Charlton and
144 Polvani 2007). Figure S1 shows the temporal evolution of the zonal-mean zonal wind at 60° N
145 and 10 hPa for 2018 SSW event. To diagnose stratospheric intrusions, we use potential vorticity
146 (PV) as a dynamical proxy associated for Rossby-wave breaking (RWB) in the upper
147 troposphere. A PV value greater than 2 PVU in the upper troposphere is taken as an indicator of
148 a stratospheric intrusion (e.g., Holton et al., 1995; Stohl et al., 2003).

149 **2.2 Computation of ozone radiative forcing**

150 The ozone radiative forcing (RF) is estimated using an ozone radiative kernel method
151 (Skeie et al., 2020). The radiative kernel is constructed using the University of Oslo radiative
152 transfer model (Myhre et al., 2011) by perturbing the ozone layer-by-layer. Temperature, water
153 vapour, and clouds are incorporated into the model from ECMWF's forecast for the year 2003
154 and applied as monthly averages. The model calculates radiative forcing using a broad-band

155 scheme for longwave radiation (Myhre and Stordal, 1997) and the DIScrete Ordinate Radiative
156 Transfer (DISORT) code for shortwave radiation (Stamnes et al., 1988). Previous studies have
157 shown that the ozone radiative forcing estimates from the radiative kernel technique and a
158 radiative transfer model agree within 0.01 W.m^{-2} globally (Iglesias-Suarez et al., 2018). Before
159 applying the kernel, the ERA5 ozone data are linearly interpolated to the kernel resolution ($\sim 5.6^\circ$
160 $\times 5.6^\circ$ horizontal, with 60 vertical levels). The interpolated ozone fields are first converted into
161 layer wise partial column amounts in Dobson units (DU) following Ziemke et al. (2001). Ozone
162 anomalies in DU are then computed from the non-SSW climatology at each grid point. These
163 layer wise DU anomalies are multiplied by the long-wave instantaneous clear-sky ozone kernel
164 ($\text{W.m}^{-2}.\text{DU}^{-1}$), which gives the change in top-of-atmosphere (TOA) long-wave radiative flux per
165 DU of ozone change in each layer. Following Shell et al. (2008), we calculate the instantaneous
166 ozone RF by vertically summing the layer wise TOA contributions from the UTLS and the total
167 atmosphere.

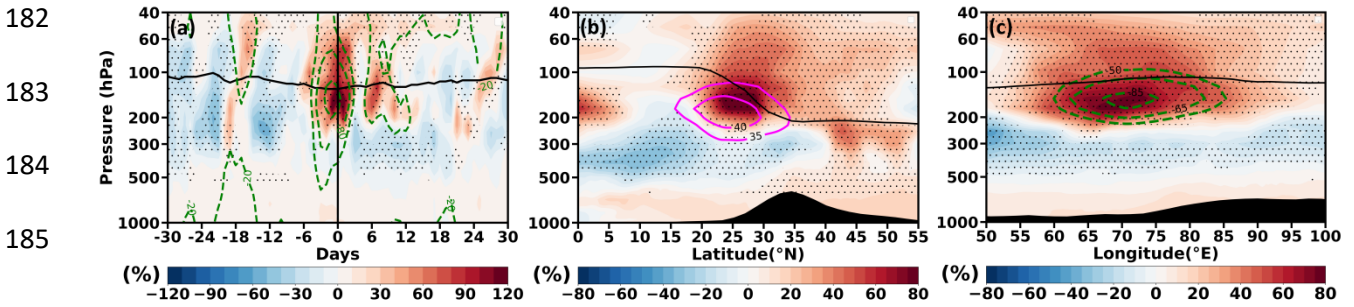
168 **2.3 Dynamical changes in PV during the 2018 event**

169 The time evolution of the vortex structure depicted by PV at 10 hPa for ± 30 days around
170 the 2018 SSW onset is shown in Fig. S2. As the SSW event approaches, the vortex begins to
171 elongate and become asymmetrical due to the influence of planetary wave activity propagating
172 upward from the troposphere; such deformation of the vortex was reported in the past (e.g.,
173 Baldwin et al., 2021). On the onset day (12 February), the vortex splits into two high-PV lobes,
174 one positioned over North America and another over Eurasia (Fig. S2h). Following the onset,
175 smaller vortices exhibit swirling and filamentation, with the Eurasian lobe drifting westward.
176 Earlier, de la Camara et al. (2018) demonstrated that planetary-scale wave breaking intensifies
177 mixing and facilitates the diffusion of PV from the vortex by elongating and stirring the PV

178 fields. These PV variations align with changes in GPH and ozone fields (e.g., Baldwin et al.,
 179 2021), emphasising stratospheric circulation changes (Fig. S2).

180 **3. Results**

181 **3.1 February 2018 SSW case: UTLS ozone variation**



186 **Figure 1.** (a) Temporal evolution of vertical ozone anomalies over the South Asian region (65-
 187 90°E, 20-35°N) from 30 days before to 30 days after the onset for the 2018 event. (b) Latitude-
 188 pressure section of ozone anomalies averaged over South Asia (65 - 90°E) for ± 6 days around
 189 the onset for 2018 SSW event. (c) is the same as that of (b) but represents longitude variations of
 190 vertical ozone anomalies averaged over South Asia (20-35°N). The horizontal and the vertical
 191 solid black line in (a) represent 380 K potential temperature isotherm and the onset day,
 192 respectively. Magenta solid contour lines in (b) represent the mean zonal wind and green dashed
 193 contour lines in (a) and (c) represent the GPH anomaly. Solid black lines in panels (b-c)
 194 represent the tropopause. Black dots indicate a region of 95% confidence level (Figure created
 195 using Python software).

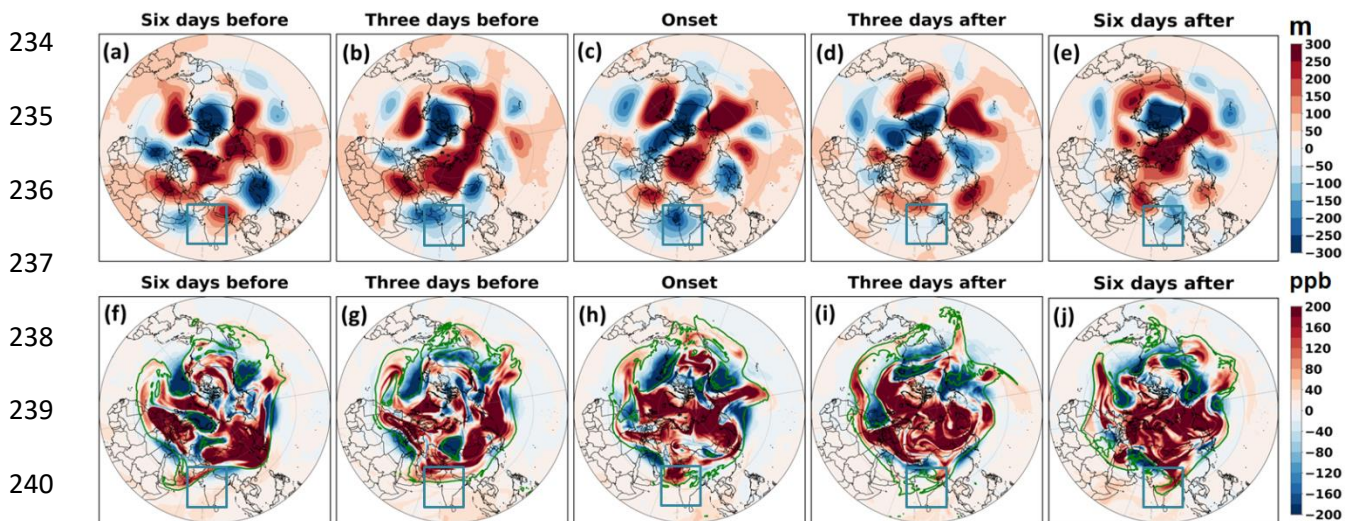
196 In this section, we discuss the ozone enhancement in the UTLS over South Asia
 197 associated with the 2018 SSW event and the possible mechanism responsible. Figures 1a show
 198 the temporal evolution of vertical ozone anomalies averaged over South Asia for the 2018 SSW
 199 event. There is a large ozone enhancement in the UTLS, with values $>80\%$ (>150 ppb) in 2018
 200 within ± 6 days around the SSW-onset. Figure 1a indicates that the ozone enhancements in the
 201 UTLS region are episodic and coincide with negative geopotential height (GPH) anomalies.
 202 Since the most pronounced ozone enhancement in the UTLS is observed within ± 6 days around
 203 the SSW onset, all subsequent analyses in this study are performed for this time period. The
 204 latitude–pressure (Fig. 1b) and longitude–pressure (Fig. 1c) cross-sections of ozone anomalies
 205 show large ozone enhancement for ± 6 days around the onset in the UTLS over South Asia,

206 exceeding 60% (>80 ppb). Interestingly, a peak in ozone enhancement is seen at the subtropical
207 jet core (Fig.1b). This suggests the role of the subtropical jet causing ozone enhancement in the
208 upper troposphere over South Asia (discussed in section 3.1.1). The strong negative GPH
209 anomaly (indicating a low-pressure area) coincident with large ozone enhancements, provides
210 evidence of stratospheric intrusions occurring during the 2018 SSW event (Fig. 1c). Past
211 literature reports ozone enhancements in the polar region associated with SSW (e.g., Baldwin et
212 al., 2021); however, high ozone enhancement in the UTLS over the South Asian region
213 underscores the unique regional impacts of SSWs.

214 **3.1.1 Causative Mechanisms for Changes in UTLS Ozone**

215 In this section, we discuss the possible mechanism responsible for the ozone
216 enhancement in the UTLS over South Asia associated with the 2018 SSW event. Several studies
217 have shown that SSW-related planetary wave disturbances occur across a deep layer of the
218 stratosphere (e.g., McIntyre, 1982; McIntyre and Palmer, 1983; Albers et al., 2016). These
219 disturbances, which are strong in the mid-to-upper stratosphere, extend downward and disrupt
220 horizontal flows in the upper troposphere (200 hPa) (Albers et al., 2016). We analysed GPH
221 anomalies at 200 hPa to understand the coupling between the stratosphere and the upper
222 troposphere. Figure 2 illustrates the evolution of GPH and ozone anomalies at 200 hPa for ± 6
223 days around the SSW onset (Feb. 12, 2018). The pattern of high and low GPH anomalies in the
224 subtropical region (15-40°N) shown in Fig. 2a-e indicates the presence of synoptic-scale Rossby
225 waves in the upper troposphere. Rossby wave breaking (RWB) is characterised by large
226 filaments of high-potential vorticity (PV) air extending towards the equator. Such quasi-
227 isentropic equatorward excursions can cause irreversible ozone intrusion from the lower
228 stratosphere into the upper troposphere (e.g., Holton et al., 1995; Waugh and Polvani, 2000;

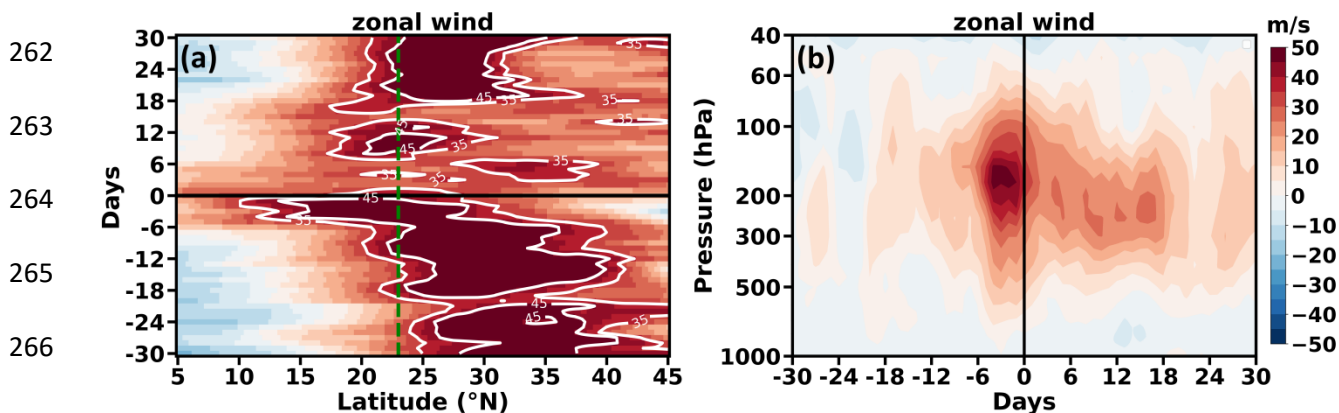
229 Albers et al., 2016). The 2 PVU contour lines and ozone anomaly maps at 200 hPa depicted in
 230 Fig. 2f-j show clear indications of ozone intrusions penetrating deep into the tropics, particularly
 231 over South Asia. The low GPH anomaly over South Asia (Figs. 2a-e) indicates a deepening
 232 trough associated with the eastward propagation of Rossby waves, facilitating enhanced
 233 stratospheric intrusions (Figs. 2f-j).



241 **Figure 2.** Spatial map of (a-e) GPH anomaly at 200 hPa, (f-j) ozone anomaly at 200 hPa from 6
 242 days before to 6 days after the onset of the 2018 SSW event, along with 2 PVU contour (green
 243 solid line), shown at 3-day intervals. The inside square box represents the South Asian region
 244 considered for the present study (Figure created using Python software).

245 RWB facilitates the stripping of stratospheric air (indicated by the 2 PVU contour) along
 246 the eastern flank of an anticyclonic centre (positive GPH anomaly, Fig. 2a–e) over the South
 247 Asian region, causing large ozone enhancements (Fig. 2f–j). Figures 2f–j clearly show that these
 248 episodic intrusions cause large ozone enhancements >150 ppb (>80%) over South Asia. Since
 249 the location and strength of the subtropical jet set the refractive waveguide and the location of
 250 wave breaking, we next diagnose the jet’s evolution during this period (Hoskins & Ambrizzi
 251 1993; Hitchman & Huesmann 2007). Figure 3 displays the latitude-time Hovmöller diagrams of
 252 zonal wind at 200 hPa and the time-altitude section around the onset over the south Asian region.

253 Figure 3 clearly shows how the jet shifted and intensified near 200 hPa around onset, creating the
 254 background flow conducive to the RWB and ozone intrusions seen in Fig. 2. The time evolution
 255 of zonal winds depicted in Figure 3a shows that thirty days before the onset, the subtropical jet
 256 core is positioned over the northern part of the Indian subcontinent, but migrates equatorward
 257 (south of 23°N) more prominently for ± 6 days around the onset. The vertical variation of zonal
 258 wind clearly depicts the intensification of westerly wind over the Indian region around 200 hPa
 259 close to the onset day, facilitating Rossby wave breaking (Fig. 3b). The strength of zonal wind is
 260 strong within ± 6 days around the onset, causing higher ozone intrusions during this period (see
 261 Figs. 1b and 3b).



267 **Figure 3.** (a) Latitude-time plot of zonal wind averaged over South Asia (65° - 90° E) at 200
 268 hPa. (b) Temporal evolution of vertical zonal wind averaged over the South Asian region (65° -
 269 90° E, 10° - 20° N) for ± 30 days around the onset of the 2018 SSW event. The horizontal dashed
 270 line in (a) and the vertical solid line in (b) represent the onset day. The vertical dashed line in (a)
 271 represents 23°N. (Figure created using Python software).

272 The observed equatorward shift of the subtropical jet during the 2018 SSW may also be
 273 influenced by the concurrent phase of the Quasi-Biennial Oscillation (QBO) (White et al., 2016;
 274 Lachmy et al., 2014; Li et al., 2023). Notably, the February 2018 SSW took place during a
 275 westerly phase of the QBO at 50 hPa in the tropics (Butler et al., 2020). Earlier studies (Park et
 276 al., 2021) have already reported an equatorward shift of subtropical jet over the East Asia–North
 277 Pacific region during the westerly phase of QBO. However, our analysis reveals a similar

278 equatorward displacement of the subtropical jet over South Asia during SSWs (Fig. 3a),
279 coinciding with the westerly QBO phase. During the westerly QBO, the associated secondary
280 circulation warms the equatorial lower stratosphere and cools the subtropics, sharpening and
281 shifting the UTLS meridional temperature gradient equatorward (e.g., Hitchman et al., 2021). By
282 thermal-wind balance, this strengthens upper-tropospheric westerlies on the equatorward flank
283 and displaces the subtropical jet equatorward over South Asian longitudes, favouring subtropical
284 wave guidance, RWB, and PV-streamer intrusions (Homeyer & Bowman, 2013; Albers et al.,
285 2016). Additionally, previous studies have shown that the westerly phase of QBO (WQBO) is
286 associated with a lowering of the tropopause (Collimore et al., 2003; Kumar et al., 2014). This
287 lowering perturbs the subtropical waveguide structure and enhances tropopause fold activity
288 (Kumar et al., 2020), thereby increasing the frequency of Rossby wave breaking and
289 strengthening stratosphere–troposphere exchange. All these supports for the link between QBO-
290 SSW conditions and the equatorward shift of the subtropical jet, along with lowering of the
291 tropopause height and increased RWB frequency over South Asia.

292 **3.2 Composite UTLS Ozone Response during all SSW Events**

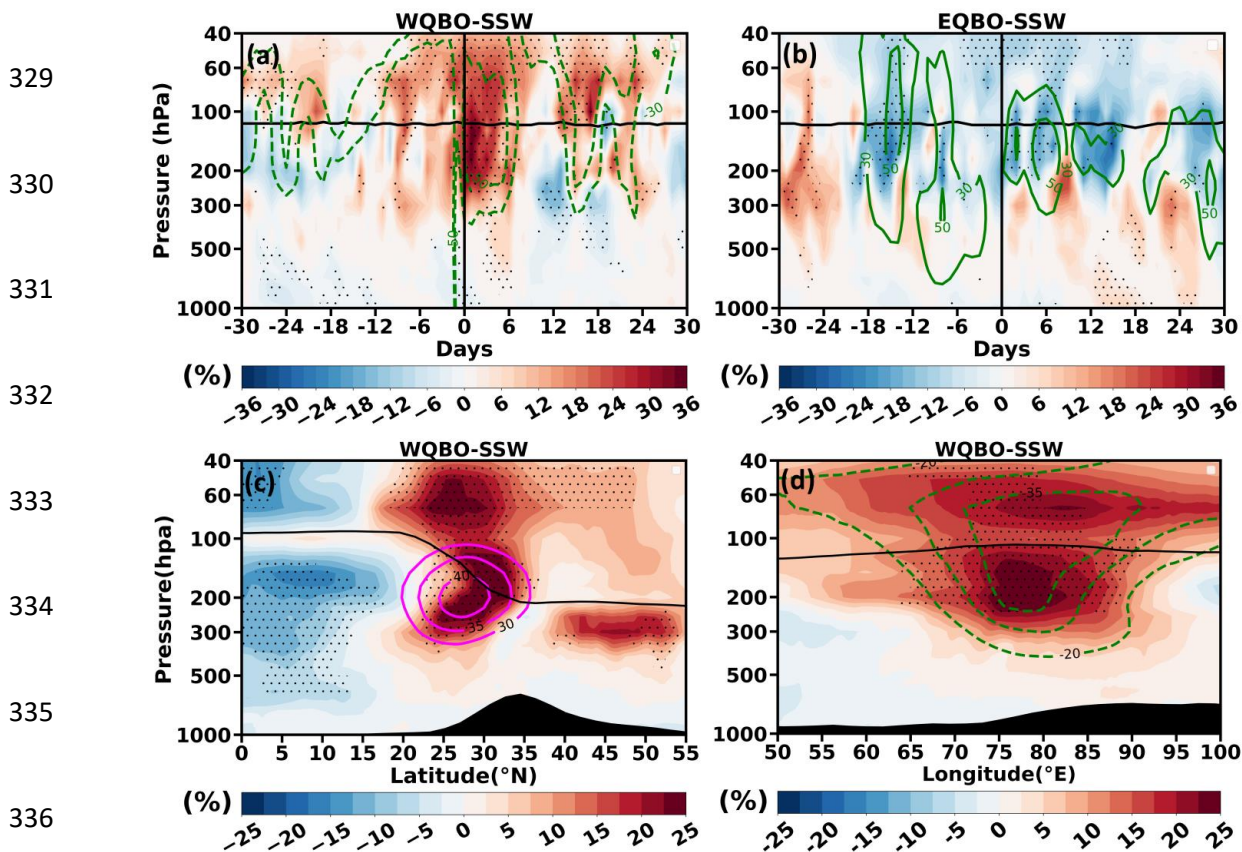
293 Further, we investigate the twenty-seven major SSW events from 1962 to 2017, to
294 examine their influence on ozone variability in the upper troposphere over the South Asian
295 region. A detailed examination of individual SSW events revealed that ozone intrusions during
296 some SSW events extend deeper and farther equatorward compared to others. Our analysis
297 shows that, as in the 2018 case, SSW coinciding with the westerly phase of QBO (fifteen out of
298 twenty-seven major SSW, WQBO-SSW) are associated with deeper and equatorward intrusion
299 of ozone compared to those SSW coinciding with the Easterly phase of QBO (twelve out of
300 twenty-seven, EQBO-SSW). Table 1 lists all the major SSW events considered in this study.

301 **Table 1.** List of all major SSW events from 1962 to 2018 considered for the present analysis
 302 alongside their onset dates and QBO phases at 70 hPa.

Year	Onset day	QBO Phase
1963	28 January	Westerly
1966	23 February	Easterly
1968	7 January	Westerly
1969	13 March	Easterly
1970	2 January	Westerly
1971	18 January	Easterly
1973	31 January	Easterly
1977	9 January	Westerly
1979	22 February	Westerly
1980	29 February	Easterly
1981	4 March	Westerly
1984	24 February	Westerly
1985	1 January	Easterly
1987	23 January	Westerly
1988	14 March	Westerly
1989	21 February	Westerly
1999	26 February	Easterly
2000	20 March	Westerly
2001	11 February	Westerly
2003	18 January	Westerly
2004	5 January	Easterly
2006	21 January	Easterly
2007	24 February	Westerly
2008	22 February	Easterly
2009	24 January	Easterly
2010	9 February	Westerly
2013	6 January	Easterly
2018	12 February	Westerly

314 Previous studies have shown that the QBO phase can modulate the dynamical coupling
 315 between the stratosphere and troposphere during SSWs (Remya et al, 2023), influencing the
 316 extent of ozone transport into the upper troposphere (Zhang et al., 2021). Our analysis shows
 317 that, during the composite WQBO-SSW events, ozone intrudes down to 400 hPa, with anomalies
 318 exceeding 30% (over 80 ppb) within ± 6 days of the onset (Fig. 4a). On the other hand, during the
 319 composite EQBO-SSW events, no significant ozone intrusion is evident within the same period

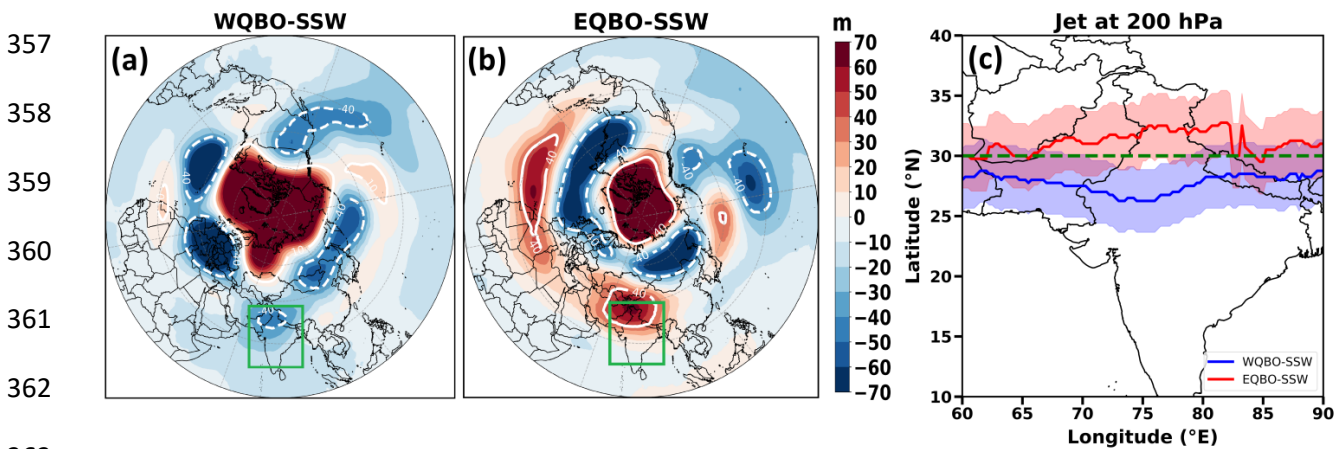
320 (Fig. 4b). The latitude–pressure (Fig. 4c) and longitude–pressure (Fig. 4d) sections further reveal
 321 enhanced ozone in the UTLS within ± 6 days over South Asia, with anomalies exceeding 20%
 322 (>60 ppb). As seen earlier (Fig. 1b-c), the maximum ozone enhancement in the WQBO–SSW
 323 composite is located near the subtropical jet core (Fig. 4c) along with a strong negative GPH
 324 anomaly (Fig. 4d), indicating that jet dynamics and troughing play a key role in modulating
 325 UTLS ozone responses during WQBO-SSW. However, the amplitude of ozone enhancement in
 326 the UTLS is smaller in the composite of all WQBO-SSW than in 2018. This subdued effect is
 327 due to averaging across multiple episodic events occurring at different times within ± 6 days
 328 around the SSW onset.



337 **Figure 4:** Temporal evolution of vertical ozone anomalies averaged over the South Asian region
 338 ($65\text{-}90^{\circ}\text{E}$, $20\text{-}35^{\circ}\text{N}$) from 30 days before to 30 days after the onset for (a) WQBO-SSW and (b)
 339 EQBO-SSW. (c) Latitude-pressure cross-section of ozone anomalies averaged over South Asia
 340 ($65 - 90^{\circ}\text{E}$) for ± 6 days around all the WQBO-SSW onsets. (d) is the same as that of (c) but
 341 represents the longitude variation of vertical ozone anomalies averaged over South Asia ($20 -$

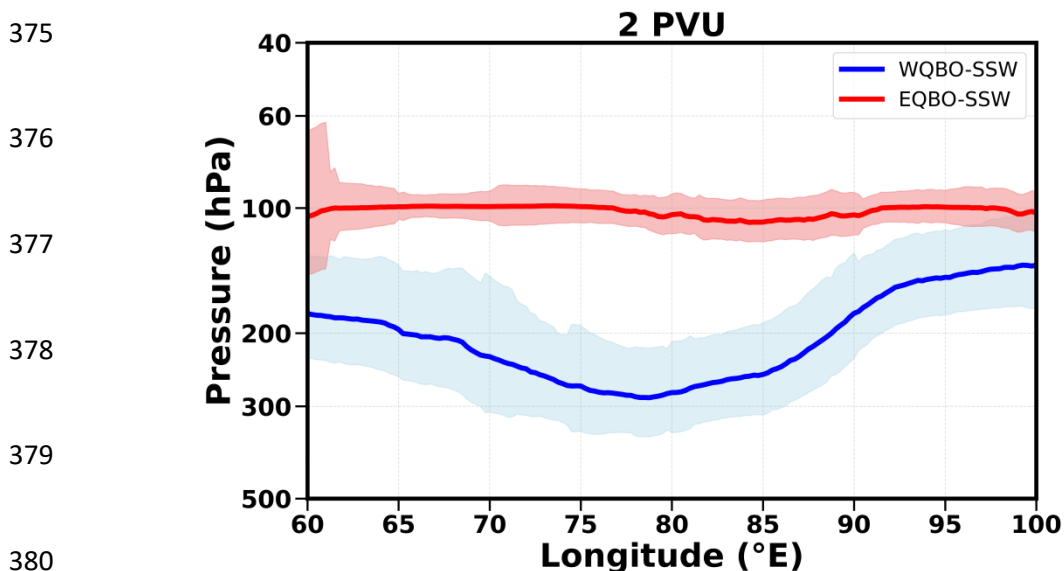
342 35°N). The horizontal solid line in (a-b) represents a 380 K potential temperature isoline, and the
 343 vertical solid line in (a-b) represents the onset day. Magenta contour lines in (c) represent the
 344 mean zonal wind, and dashed green contour lines in (a,d) represent the negative GPH anomaly
 345 and solid green contour lines in (b) represent the positive GPH anomaly. Solid black lines in (c-
 346 d) represent the tropopause. Black dots indicate a region of 95% confidence level (Figure created
 347 using Python software).

348 Further, we analysed the synoptic wave structure prevailing in the upper troposphere for
 349 WQBO-SSW and EQBO-SSW composites within ± 6 days around the onset, using the 200 hPa
 350 GPH anomaly as a proxy (Figs. 5a–b). The alternating trough–ridge patterns in GPH over the
 351 subtropics indicate synoptic-scale Rossby waves in the upper troposphere. During the SSWs
 352 associated with the westerly phase of the QBO, a pronounced low GPH anomaly is observed
 353 over the South Asian region (Fig. 5a), whereas high GPH dominates during the SSWs coinciding
 354 with the easterly phase (Fig. 5b). The anomalous low over South Asia during WQBO-SSW
 355 events indicates a deepening of the upper-tropospheric trough, which favours the likelihood of
 356 stratospheric intrusions into the upper troposphere.



364 **Figure 5.** Spatial map of GPH anomaly for (a) WQBO-SSW and (b) EQBO-SSW and (c) jet
 365 core at 200 hPa averaged for ± 6 days around the onset. White solid and dashed contour line in
 366 (a-b) indicates positive and negative GPH anomaly. The square box in (a-b) represents the South
 367 Asian region considered for the present study. Blue line and red line in (c) represents jet core for
 368 westerly phase and easterly phase of QBO respectively. The shading in (c) represents standard
 369 error. (Figure created using Python software).

370 Further, we show the composite position of the subtropical jet core within ± 6 days around
 371 the SSW onset. Figure 5c shows that during SSWs coinciding with the westerly phase of the
 372 QBO, the subtropical jet shifts equatorward, with the jet core (blue lines) located south of 30°N
 373 over the South Asian region. Whereas, during the easterly QBO phase, the jet core (red line)
 374 remains north of 30°N . (detailed mechanism discussed in the section 3.1.1).



381 **Figure 6.** Longitude–pressure cross section of 2PVU line averaged over South Asia ($20\text{--}35^\circ\text{N}$)
 382 for WQBO–SSW and EQBO–SSW composites within ± 6 days around the onset. The shading
 383 represents standard error. (Figure created using Python software).

384 The PV–based RWB diagnostics to identify the stratospheric intrusion during both
 385 WQBO–SSW and EQBO–SSW composites are shown in Figure 6. For each event, the day of
 386 maximum intrusion within ± 6 days around the onset was chosen to capture the most
 387 representative feature, as full averaging over the period tends to smooth out the signal. The
 388 longitude–pressure cross section (Fig. 6) shows that during the WQBO–SSW composite, the 2
 389 PVU contour extends farther downward into the upper troposphere, indicating stronger PV
 390 intrusions. On the other hand, during EQBO–SSW events, the 2 PVU contour remains confined
 391 to higher altitudes, suggesting weaker intrusions (detailed mechanism discussed in section 3.1.1).

392 Taken together, the equatorward shift of subtropical jet over the South Asian region, persistent
393 negative GPH anomaly (trough), and downward extending PV intrusions all point towards a
394 strengthening of a stratospheric intrusion during the SSWs concurrent with westerly phase of
395 QBO.

396 **3.3 Radiative Forcing of ozone associated with WQBO-SSWs over the South Asian region**

397 Further, we assessed instantaneous radiative forcing at the top of the atmosphere (TOA)
398 due to ozone enhancements in the UTLS and total-column over the South Asian region
399 associated with WQBO-SSW events. The instantaneous RF is computed for ± 6 days around the
400 onset. Due to the ozone enhancements in the UTLS, a positive radiative forcing at the top of the
401 atmosphere of $0.25 \pm 0.18 \text{ W.m}^{-2}$ is observed in the 2018 SSW event, while the WQBO-SSW
402 composite exhibits a forcing of $0.09 \pm 0.05 \text{ W.m}^{-2}$. In contrast, due to the total-column ozone
403 changes, a radiative forcing at the TOA of $0.28 \pm 0.19 \text{ W.m}^{-2}$ for the 2018 event and 0.17 ± 0.05
404 W.m^{-2} for the composite is observed. These results highlight the significant role of WQBO-SSW
405 events in modulating the radiative balance in the troposphere, particularly in the UTLS over
406 South Asia.

407 **4. Conclusions**

408 Using the ERA5 reanalysis (1962–2018), we investigated the impact of sudden
409 stratospheric warmings (SSWs) on ozone variations in the UTLS (300–50 hPa) over South Asia.
410 Unlike prior global analyses, we demonstrate that SSWs coinciding with the westerly phase of
411 QBO (WQBO-SSW) lead to a substantial enhancement in UTLS ozone and radiative forcing
412 over the South Asian region, whereas SSWs associated with the easterly phase of QBO (EQBO-
413 SSW) do not. Our analysis shows that, unlike high latitudes, the South Asian response is not a
414 direct downward influence. These low-latitude impacts are mediated by Rossby-wave dynamics.

415 In particular, Rossby-wave breaking (RWB) and PV-streamer intrusions develop with the
416 equatorward meandering of the subtropical jet.

417 We find that SSWs coinciding with the westerly phase of the QBO (WQBO-SSW) are
418 associated with an equatorward shift (south of 30°N over South Asia) of the subtropical jet and
419 lowering of tropopause which intensifies RWB and the largest UTLS ozone anomalies over
420 South Asia. An enhancement in ozone anomalies (ranging from 30 to 80% or 80 to 150 ppb for
421 composite and 2018) in the UTLS is noted during the WQBO-SSW years relative to the non-
422 SSW calendar-day climatology within ± 6 days of onset. This ozone enhancement in the UTLS
423 during WQBO-SSW events contributes an instantaneous radiative forcing at the top of the
424 atmosphere of $0.25 \pm 0.18 \text{ W.m}^{-2}$ for the 2018 and $0.09 \pm 0.05 \text{ W.m}^{-2}$ during the composite.
425 Whereas due to total-column ozone changes, computed instantaneous RF at the top of the
426 atmosphere is $0.28 \pm 0.19 \text{ W.m}^{-2}$ for 2018 and $0.17 \pm 0.05 \text{ W.m}^{-2}$ for the WQBO-SSW
427 composite.

428 This large increase in radiative forcing produces positive feedback on the warming
429 climate of this region. Ozone intrusions are warranted to elevate pollution effects and climate
430 warming, impacting people's health, the ecosystem, and the economy. The frequency of SSW is
431 projected to increase in a warming climate (Kim et al., 2017), which will further increase
432 stratospheric ozone intrusions and potentially amplify the consequences of positive feedback
433 mechanisms. Since the evolution of the polar vortex modulates subtropical Rossby-wave guides
434 that affect South Asia, these stratospheric influences must be represented in regional prediction
435 systems. We emphasise that climate models should be extended to the stratosphere, including
436 polar vortex dynamics, for accurate prediction of climate over South Asia. Earlier studies show

437 that using high-top, stratosphere-resolving models improve subseasonal-to-seasonal
438 predictability (Hardiman et al., 2012; Charlton-Perez et al., 2013; Scaife et al., 2022).

439

440 **Code and data availability**

441 The ERA5 data that support the findings of this study are openly available from
442 <https://cds.climate.copernicus.eu/> (10.24381/cds.bd0915c6). The python code used to plot figures
443 in this paper are available from <https://doi.org/10.5281/zenodo.17639489>

444 **Acknowledgements**

445 The authors thank the staff of the High Power Computing Centre (HPC) in IITM, Pune, India,
446 for providing computer resources and the team members of ERA5 for providing data. The
447 authors are thankful to three anonymous reviewers for their valuable suggestions.

448 **Author contributions**

449 Conceptualisation: S.F. Supervision: SF, MH, RF Investigation and methodology: SC, SR, VS,
450 and PC. Writing: all authors.

451 **Competing interests**

452 At least one of the (co-)authors is a member of the editorial board of Atmospheric Chemistry and
453 Physics.

454

455

456

457

458

459

460 **References:**

- 461 Albers, J. R., Kiladis, G. N., Birner, T. and Dias, J.: Tropical upper-tropospheric potential
462 vorticity intrusions during sudden stratospheric warmings, *Journal of the Atmospheric*
463 *Sciences*, 73(6), 2361–2384, doi:10.1175/jas-d-15-0238.1, 2016.
- 464 Baldwin, M. P. and Dunkerton, T. J.: Stratospheric harbingers of anomalous weather regimes,
465 *Science*, 294(5542), 581–584, doi:10.1126/science.1063315, 2001.
- 466 Baldwin, M. P., Domeisen, D. I. V., Hegglin, M. I., Garny, H., Garfinkel, C. I., Langematz, U.,
467 Charlton-Perez, A. J., Butchart, N., Gerber, E. P., Birner, T., Butler, A. H., Ayarzagüena, B.,
468 and Pedatella, N. M.: Sudden Stratospheric Warmings, *Reviews of Geophysics*, 59,
469 <https://doi.org/10.1029/2020rg000708>, 2021.
- 470 Butler, A. H., Seidel, D. J., Hardiman, S. C., Butchart, N., Birner, T. and Match, A.: Defining
471 sudden stratospheric warmings, *Bulletin of the American Meteorological Society*, 96(11),
472 1913–1928, doi:10.1175/bams-d-13-00173.1, 2015.
- 473 Butler, A. H., Lillo, S. P., Long, C. S., Lee, S. H., and Lawrence, Z. D.: Differences between the
474 2018 and 2019 stratospheric polar vortex split events, *Quarterly Journal of the Royal*
475 *Meteorological Society*, 146, 3503–3521, <https://doi.org/10.1002/qj.3858>, 2020.
- 476 Charlton, A. J. and Polvani, L. M.: A new look at stratospheric sudden warmings. part I:
477 Climatology and modeling benchmarks, *Journal of Climate*, 20(3), 449–469,
478 doi:10.1175/jcli3996.1, 2007.
- 479 Charlton-Perez, A. J., Polvani, L. M., Austin, J. and Li, F.: The frequency and dynamics of
480 stratospheric sudden warmings in the 21st century, *Journal of Geophysical Research:*
481 *Atmospheres*, 113(D16), doi:10.1029/2007jd009571, 2008.
- 482 Charlton-Perez, A. J., Baldwin, M. P., Shaw, T. A., Hardiman, S., Polvani, L., Shindell, D.,
483 Yoden, S., Gerber, E. P., Manzini, E., Calvo, N., Yukimoto, S., Lott, F., Davis, N. A., Black,
484 R. X., Butler, A. H., Krüger, K., Son, S., Kim, J., Lee, Y., Mcdaniel, B. A., Reichler, T.,
485 Christiansen, B., Watanabe, S., Toohey, M., Sigmond, M., Gillett, N., Wilcox, L., and
486 Birner, T.: On the lack of stratospheric dynamical variability in low-top versions of the
487 CMIP5 models, *Journal of Geophysical Research: Atmospheres*, 118, 2494–2505,
488 <https://doi.org/10.1002/jgrd.50125>, 2013.
- 489 Collimore, C. C., Huesmann, A., Martin, D. W., Hitchman, M. H., and Waliser, D. E.: On The
490 Relationship between the QBO and Tropical Deep Convection, *Journal of Climate*, 16,
491 2552–2568, [https://doi.org/10.1175/1520-0442\(2003\)016<2552:otrbtq>2.0.co;2](https://doi.org/10.1175/1520-0442(2003)016<2552:otrbtq>2.0.co;2), 2003.

- 492 Dewan, S. and Lakhani, A.: Tropospheric ozone and its natural precursors impacted by climatic
493 changes in emission and dynamics, *Frontiers in Environmental Science*, 10,
494 doi:10.3389/fenvs.2022.1007942, 2022.
- 495 de la Cámara, A., Abalos, M. and Hitchcock, P.: Changes in stratospheric transport and mixing
496 during sudden stratospheric warmings, *Journal of Geophysical Research: Atmospheres*,
497 123(7), 3356–3373, doi:10.1002/2017jd028007, 2018.
- 498 Domeisen, D. I. and Butler, A. H.: Stratospheric drivers of extreme events at the Earth’s surface,
499 *Communications Earth & Environment*, 1(1), doi:10.1038/s43247-020-00060-z, 2020.
- 500 Domeisen, D. I., Grams, C. M. and Papritz, L.: The role of North Atlantic–European weather
501 regimes in the surface impact of sudden stratospheric warming events, *Weather and Climate*
502 *Dynamics*, 1(2), 373–388, doi:10.5194/wcd-1-373-2020, 2020.
- 503 Fadnavis, S., Chakraborty, T., and Beig, G.: Seasonal stratospheric intrusion of ozone in the
504 upper troposphere over India, *Annales Geophysicae*, 28, 2149–2159,
505 <https://doi.org/10.5194/angeo-28-2149-2010>, 2010.
- 506 Fadnavis, S., Wienhold, F. G., Müller, R., Oelsner, P., Vogel, B., Naja, M., Sonbawne, S.,
507 Dirksen, R., Sagalgile, A., and Peter, T.: Comparison of ozonesonde measurements in the
508 upper troposphere and lower Stratosphere in Northern India with reanalysis and chemistry-
509 climate-model data, *Scientific Reports*, 13, <https://doi.org/10.1038/s41598-023-34330-5>,
510 2023.
- 511 Feng, Z., Agathokleous, E., Yue, X., Oksanen, E., Paoletti, E., Sase, H., Gandin, A., Koike, T.,
512 Calatayud, V., Yuan, X., Liu, X., De Marco, A., Jolivet, Y., Kontunen-Soppela, S., Hoshika,
513 Y., Saji, H., Li, P., Li, Z., Watanabe, M. and Kobayashi, K.: Emerging challenges of ozone
514 impacts on Asian plants: Actions are needed to protect ecosystem health, *Ecosystem Health*
515 *and Sustainability*, 7(1), doi:10.1080/20964129.2021.1911602, 2021.
- 516 Fleming, Z. L., Doherty, R. M., von Schneidmesser, E., Malley, C. S., Cooper, O. R., Pinto, J.
517 P., Colette, A., Xu, X., Simpson, D., Schultz, M. G., Lefohn, A. S., Hamad, S., Moolla, R.,
518 Solberg, S. and Feng, Z.: Tropospheric Ozone Assessment Report: Present-day ozone
519 distribution and trends relevant to human health, *Elementa: Science of the Anthropocene*, 6,
520 doi:10.1525/elementa.273, 2018.
- 521 Fowler, D., Pilegaard, K., Sutton, M. A., Ambus, P., Raivonen, M., Duyzer, J., Simpson, D.,
522 Fagerli, H., Fuzzi, S., Schjoerring, J. K., Granier, C., Neftel, A., Isaksen, I. S. A., Laj, P.,
523 Maione, M., Monks, P. S., Burkhardt, J., Daemmgen, U., Neiryneck, J., Personne, E.,
524 Wichink-Kruit, R., Butterbach-Bahl, K., Flechard, C., Tuovinen, J. P., Coyle, M., Gerosa,
525 G., Loubet, B., Altimir, N., Gruenhage, L., Ammann, C., Cieslik, S., Paoletti, E., Mikkelsen,

526 T. N., Ro-Poulsen, H., Cellier, P., Cape, J. N., Horváth, L., Loreto, F., Niinemets, Palmer, P.
527 I., Rinne, J., Misztal, P., Nemitz, E., Nilsson, D., Pryor, S., Gallagher, M. W., Vesala, T.,
528 Skiba, U., Brüggemann, N., Zechmeister-Boltenstern, S., Williams, J., O'Dowd, C.,
529 Facchini, M. C., de Leeuw, G., Flossman, A., Chaumerliac, N. and Erisman, J. W.:
530 Atmospheric composition change: Ecosystems–atmosphere interactions, *Atmospheric*
531 *Environment*, 43(33), 5193–5267, doi:10.1016/j.atmosenv.2009.07.068, 2009.

532 Hall, R. J., Mitchell, D. M., Seviour, W. J. and Wright, C. J.: Tracking the stratosphere-to-
533 surface impact of sudden stratospheric warmings, *Journal of Geophysical Research:*
534 *Atmospheres*, 126(3), doi:10.1029/2020jd033881, 2021.

535 Hardiman, S. C., Butchart, N., Hinton, T. J., Gray, L. J., and Osprey, S. M.: The Effect of a
536 Well-Resolved Stratosphere on Surface Climate: Differences between CMIP5 Simulations
537 with High and Low Top Versions of the Met Office Climate Model, *Journal of Climate*, 25,
538 7083–7099, <https://doi.org/10.1175/jcli-d-11-00579.1>, 2012.

539 Hersbach, H., Bell, B., Berrisford, P., Hirahara, S., Horányi, A., Muñoz-Sabater, J., Nicolas, J.,
540 Peubey, C., Radu, R., Schepers, D., Simmons, A., Soci, C., Abdalla, S., Abellan, X.,
541 Balsamo, G., Bechtold, P., Biavati, G., Bidlot, J., Bonavita, M., De Chiara, G., Dahlgren, P.,
542 Dee, D., Diamantakis, M., Dragani, R., Flemming, J., Forbes, R., Fuentes, M., Geer, A.,
543 Haimberger, L., Healy, S., Hogan, R. J., Hólm, E., Janisková, M., Keeley, S., Laloyaux, P.,
544 Lopez, P., Lupu, C., Radnoti, G., de Rosnay, P., Rozum, I., Vamborg, F., Villaume, S. and
545 Thépaut, J.: The ERA5 global reanalysis, *Quarterly Journal of the Royal Meteorological*
546 *Society*, 146(730), 1999–2049, doi:10.1002/qj.3803, 2020.

547 Hitchman, M. H. and Huesmann, A. S.: A Seasonal Climatology of Rossby Wave Breaking in
548 the 320–2000-K Layer, *Journal of the Atmospheric Sciences*, 64, 1922–1940,
549 <https://doi.org/10.1175/jas3927.1>, 2007.

550 Hitchman, M. H., Tegtmeier, S., Yoden, S., Haynes, P. H., and Kumar, V.: An Observational
551 History of the Direct Influence of the Stratospheric Quasi-biennial Oscillation on the
552 Tropical and Subtropical Upper Troposphere and Lower Stratosphere, *Journal of the*
553 *Meteorological Society of Japan. Ser. II*, 99, 239–267, [https://doi.org/10.2151/jmsj.2021-](https://doi.org/10.2151/jmsj.2021-012)
554 012, 2021.

555 Holton, J. R., Haynes, P. H., McIntyre, M. E., Douglass, A. R., Rood, R. B. and Pfister, L.:
556 Stratosphere-Troposphere exchange, *Reviews of Geophysics*, 33(4), 403–439,
557 doi:10.1029/95rg02097, 1995.

558 Homeyer, C. R. and Bowman, K. P.: Rossby Wave Breaking and Transport between the Tropics
559 and Extratropics above the Subtropical Jet, *Journal of the Atmospheric Sciences*, 70, 607–
560 626, <https://doi.org/10.1175/jas-d-12-0198.1>, 2013.

- 561 Hoskins, B. J. and Ambrizzi, T.: Rossby Wave Propagation on a Realistic Longitudinally
562 Varying Flow, *Journal of the Atmospheric Sciences*, 50, 1661–1671,
563 [https://doi.org/10.1175/1520-0469\(1993\)050<1661:rwpoar>2.0.co;2](https://doi.org/10.1175/1520-0469(1993)050<1661:rwpoar>2.0.co;2), 1993.
- 564 Iglesias-Suarez, F., Kinnison, D. E., Rap, A., Maycock, A. C., Wild, O. and Young, P. J.: Key
565 drivers of ozone change and its radiative forcing over the 21st century, *Atmospheric*
566 *Chemistry and Physics*, 18(9), 6121–6139, doi:10.5194/acp-18-6121-2018, 2018.
- 567 Kidston, J., Scaife, A. A., Hardiman, S. C., Mitchell, D. M., Butchart, N., Baldwin, M. P. and
568 Gray, L. J.: Stratospheric influence on tropospheric jet streams, storm tracks and Surface
569 Weather, *Nature Geoscience*, 8(6), 433–440, doi:10.1038/ngeo2424, 2015.
- 570 Kim, J., Park, H.-S., Son, S.-W., and Gerber, E. P.: Defining Sudden Stratospheric Warming in
571 Climate Models: Accounting for Biases in Model Climatologies, *Journal of Climate*, 30,
572 5529–5546, <https://doi.org/10.1175/jcli-d-16-0465.1>, 2017.
- 573 Kumar, V., Dhaka, S. K., Reddy, K. K., Gupta, A., Prasad, S. B. S., Panwar, V., Singh, N., Ho,
574 S.-P., and Takahashi, M.: Impact of quasi-biennial oscillation on the inter-annual variability
575 of the tropopause height and temperature in the tropics: A study using
576 COSMIC/FORMOSAT-3 observations, *Atmospheric Research*, 139, 62–70,
577 <https://doi.org/10.1016/j.atmosres.2013.12.014>, 2014.
- 578 Kumar, K. N., Sharma, S. K., Naja, M., and Phanikumar, D. V.: A Rossby wave breaking-
579 induced enhancement in the tropospheric ozone over the Central Himalayan region,
580 *Atmospheric Environment*, 224, 117356, <https://doi.org/10.1016/j.atmosenv.2020.117356>,
581 2020.
- 582 Lachmy, O and Harnik, N.: The Transition to a Subtropical Jet Regime and Its Maintenance,
583 *Journal of the Atmospheric Sciences*, 71, 1389–1409, <https://doi.org/10.1175/jas-d-13-0125.1>, 2014.
- 585 Li, H., Fan, Y., Li, Q., Ji, X., Zhang, J., and Sheng, B.: The Gravity Wave Activity during Two
586 Recent QBO Disruptions Revealed by U.S. High-Resolution Radiosonde Data, *Remote*
587 *Sensing*, 15, 472, <https://doi.org/10.3390/rs15020472>, 2023.
- 588 Li, Y., Xia, Y., Xie, F. and Yan, Y.: Influence of stratosphere-troposphere exchange on long-
589 term trends of surface ozone in CMIP6, *Atmospheric Research*, 297, 107086,
590 doi:10.1016/j.atmosres.2023.107086, 2024.
- 591 Lim, S. S., Vos, T., Flaxman, A. D., Danaei, G., Shibuya, K., Adair-Rohani, H., AlMazroa, M.
592 A., Amann, M., Anderson, H. R., Andrews, K. G., Aryee, M., Atkinson, C., Bacchus, L. J.,
593 Bahalim, A. N., Balakrishnan, K., Balmes, J., Barker-Collo, S., Baxter, A., Bell, M. L.,
594 Blore, J. D., Blyth, F., Bonner, C., Borges, G., Bourne, R., Boussinesq, M., Brauer, M.,

595 Brooks, P., Bruce, N. G., Brunekreef, B., Bryan-Hancock, C., Bucello, C., Buchbinder, R.,
596 Bull, F., Burnett, R. T., Byers, T. E., Calabria, B., Carapetis, J., Carnahan, E., Chafe, Z.,
597 Charlson, F., Chen, H., Chen, J. S., Cheng, A. T.-A., Child, J. C., Cohen, A., Colson, K. E.,
598 Cowie, B. C., Darby, S., Darling, S., Davis, A., Degenhardt, L., Dentener, F., Des Jarlais, D.
599 C., Devries, K., Dherani, M., Ding, E. L., Dorsey, E. R., Driscoll, T., Edmond, K., Ali, S. E.,
600 Engell, R. E., Erwin, P. J., Fahimi, S., Falder, G., Farzadfar, F., Ferrari, A., Finucane, M. M.,
601 Flaxman, S., Fowkes, F. G., Freedman, G., Freeman, M. K., Gakidou, E., Ghosh, S.,
602 Giovannucci, E., Gmel, G., Graham, K., Grainger, R., Grant, B., Gunnell, D., Gutierrez, H.
603 R., Hall, W., Hoek, H. W., Hogan, A., Hosgood, H. D., Hoy, D., Hu, H., Hubbell, B. J.,
604 Hutchings, S. J., Ibeanusi, S. E., Jacklyn, G. L., Jasrasaria, R., Jonas, J. B., Kan, H., Kanis, J.
605 A., Kassebaum, N., Kawakami, N., Khang, Y.-H., Khatibzadeh, S., Khoo, J.-P., et al.: A
606 comparative risk assessment of burden of disease and injury attributable to 67 risk factors
607 and risk factor clusters in 21 regions, 1990–2010: A systematic analysis for the global
608 burden of disease study 2010, *The Lancet*, 380(9859), 2224–2260, doi:10.1016/s0140-
609 6736(12)61766-8, 2012.

610 Lin, Y., Jiang, F., Zhao, J., Zhu, G., He, X., Ma, X., Li, S., Sabel, C. E. and Wang, H.: Impacts
611 of O₃ on premature mortality and crop yield loss across China, *Atmospheric Environment*,
612 194, 41–47, doi:10.1016/j.atmosenv.2018.09.024, 2018.

613 Liu, Y., Gao, S. T., Brasseur, G., Tie, X. X., Wang, H. P., Kinnison, D., and Liu, C. X.:
614 Atmospheric tracers during the 2003–2004 stratospheric warming event and impact of ozone
615 intrusions in the troposphere, *Atmospheric Chemistry and Physics*, 9, 2157–2170,
616 <https://doi.org/10.5194/acp-9-2157-2009>, 2009.

617 Lu, Q., Shi, C., Liang, Z., Wang, J., Fu, G., Guo, D., and Rao, J.: Possible influence of Sudden
618 Stratospheric Warmings on the atmospheric environment in the Beijing-Tianjin-Hebei
619 region, <https://doi.org/10.5194/acp-2022-279>, 1 June 2022.

620 Ma, X., Huang, J., Hegglin, M., Joeckel, P. and Zhao, T.: Causes of growing middle-upper
621 tropospheric ozone over the Northwest Pacific Region, doi:10.5194/egusphere-2023-2411,
622 2024.

623 McIntyre, M. E. and Palmer, T. N.: Breaking planetary waves in the stratosphere, *Nature*,
624 305(5935), 593–600, doi:10.1038/305593a0, 1983.

625 McIntyre, M. E.: How well do we understand the dynamics of stratospheric warmings?, *Journal*
626 *of the Meteorological Society of Japan. Ser. II*, 60(1), 37–65,
627 doi:10.2151/jmsj1965.60.1_37, 1982.

628 Myhre, G., & Stordal, F.: Role of spatial and temporal variations in the computation of radiative
629 forcing and GWP. *Journal of Geophysical Research: Atmospheres*, 102(D10), 11181–11200.
630 <https://doi.org/10.1029/97jd00148>, 1997.

631 Myhre, G., Shine, K. P., Rädcl, G., Gauss, M., Isaksen, I. S. A., Tang, Q., Prather, M. J.,
632 Williams, J. E., van Velthoven, P., Dessens, O., Koffi, B., Szopa, S., Hoor, P., Grewe, V.,
633 Borken-Kleefeld, J., Berntsen, T. K. and Fuglestvedt, J. S.: Radiative forcing due to changes
634 in ozone and methane caused by the transport sector, *Atmospheric Environment*, 45(2), 387–
635 394, doi:10.1016/j.atmosenv.2010.10.001, 2011.

636 Park, C., Choi, J., Son, S., and Lim, Y.: Quasi-biennial oscillation-related surface air temperature
637 change over the western North Pacific in late winter, *International Journal of Climatology*,
638 42, 4351–4359, <https://doi.org/10.1002/joc.7470>, 2021.

639 Remya, R., Manoj, M. G., and Mohanakumar, K.: Role of Quasi-Biennial oscillation on the link
640 between sudden stratospheric warming and tropical weather events, *Advances in Space*
641 *Research*, 73, 571–584, <https://doi.org/10.1016/j.asr.2023.11.006>, 2023.

642 Roy, C., Thazhe Purayil, S., and Fadnavis, S.: The stratospheric ozone rich cold intrusion during
643 El-Nino over the Indian region: implication during the Indian summer monsoon,
644 <https://doi.org/10.5194/egusphere-egu2020-937>, 2020.

645 Roy, C., Ravishankara, A. R., Newman, P. A., David, L. M., Fadnavis, S., Rathod, S. D., Lait,
646 L., Krishnan, R., Clark, H. and Sauvage, B.: Estimation of stratospheric intrusions during
647 Indian Cyclones, *Journal of Geophysical Research: Atmospheres*, 128(3),
648 doi:10.1029/2022jd037519, 2023.

649 Scaife, A. A., Charlton-Perez, A. J., Son, S.-W., Hardiman, S. C., Polvani, L., Lim, E.-P.,
650 Haynes, P., Baldwin, M. P., Shepherd, T. G., Perlwitz, J., Richter, J. H., Noguchi, S.,
651 Thompson, D. W. J., Karpechko, A. Y., Butler, A. H., Scinocca, J., Sigmond, M., Domeisen,
652 D. Shi. V., and Garfinkel, C. I.: Long-range prediction and the stratosphere, *Atmospheric*
653 *Chemistry and Physics*, 22, 2601–2623, <https://doi.org/10.5194/acp-22-2601-2022>, 2022.

654 Schimanke, S., Spanghel, T., Huebener, H. and Cubasch, U.: Variability and trends of major
655 stratospheric warmings in simulations under constant and increasing GHG concentrations,
656 *Climate Dynamics*, 40(7–8), 1733–1747, doi:10.1007/s00382-012-1530-x, 2012.

657 Shell, K. M., Kiehl, J. T. and Shields, C. A.: Using the radiative kernel technique to calculate
658 climate feedbacks in NCAR’s community atmospheric model, *Journal of Climate*, 21(10),
659 2269–2282, doi:10.1175/2007jcli2044.1, 2008.

660 Shi, Y., Evtushevsky, O., Milinevsky, G., Wang, X., Klekociuk, A., Han, W., Grytsai, A., Wang,
661 Y., Wang, L., Novosyadlyj, B., and Andrienko, Y.: Impact of the 2018 major sudden

662 stratospheric warming on weather over the midlatitude regions of Eastern Europe and East
663 Asia, *Atmospheric Research*, 297, 107112, <https://doi.org/10.1016/j.atmosres.2023.107112>,
664 2023.

665 Sigmond, M., Scinocca, J. F., Kharin, V. V. and Shepherd, T. G.: Enhanced seasonal forecast
666 skill following stratospheric sudden warmings, *Nature Geoscience*, 6(2), 98–102,
667 doi:10.1038/ngeo1698, 2013.

668 Silva, R. A., West, J. J., Zhang, Y., Anenberg, S. C., Lamarque, J.-F., Shindell, D. T., Collins,
669 W. J., Dalsoren, S., Faluvegi, G., Folberth, G., Horowitz, L. W., Nagashima, T., Naik, V.,
670 Rumbold, S., Skeie, R., Sudo, K., Takemura, T., Bergmann, D., Cameron-Smith, P., Cionni,
671 I., Doherty, R. M., Eyring, V., Josse, B., MacKenzie, I. A., Plummer, D., Righi, M.,
672 Stevenson, D. S., Strode, S., Szopa, S. and Zeng, G.: Global premature mortality due to
673 anthropogenic outdoor air pollution and the contribution of past climate change,
674 *Environmental Research Letters*, 8(3), 034005, doi:10.1088/1748-9326/8/3/034005, 2013.

675 Skeie, R. B., Myhre, G., Hodnebrog, Ø., Cameron-Smith, P. J., Deushi, M., Hegglin, M. I.,
676 Horowitz, L. W., Kramer, R. J., Michou, M., Mills, M. J., Olivie, D. J., Connor, F. M.,
677 Paynter, D., Samset, B. H., Sellar, A., Shindell, D., Takemura, T., Tilmes, S. and Wu, T.:
678 Historical total ozone radiative forcing derived from CMIP6 simulations, *npj Climate and*
679 *Atmospheric Science*, 3(1), doi:10.1038/s41612-020-00131-0, 2020.

680 SPARC Reanalysis Intercomparison Project (S-RIP) Final Report. M. Fujiwara, G.L. Manney,
681 L.J. Gray, and J.S. Wright (Eds.), SPARC Report No. 10, WCRP-17/2020, doi:
682 10.17874/800dee57d13, available at www.sparc-climate.org/publications/sparc-reports,
683 2022.

684 Stohl, A., Bonasoni, P., Cristofanelli, P., Collins, W., Feichter, J., Frank, A., Forster, C.,
685 Gerasopoulos, E., Gäggeler, H., James, P., Kentarchos, T., Kromp-Kolb, H., Krüger, B.,
686 Land, C., Meloan, J., Papayannis, A., Priller, A., Seibert, P., Sprenger, M., ... Zerefos, C.:
687 Stratosphere-Troposphere Exchange: A review, and what we have learned from Staccato.
688 *Journal of Geophysical Research: Atmospheres*, 108(D12).
689 <https://doi.org/10.1029/2002jd002490>, 2003.

690 Stamnes, K., Tsay, S.-C., Wiscombe, W. and Jayaweera, K.: Numerically stable algorithm for
691 discrete-ordinate-method radiative transfer in multiple scattering and emitting layered
692 media, *Applied Optics*, 27(12), 2502, doi:10.1364/ao.27.002502, 1988.

693 Wang, H., Lu, X., Jacob, D. J., Cooper, O. R., Chang, K.-L., Li, K., Gao, M., Liu, Y., Sheng, B.,
694 Wu, K., Wu, T., Zhang, J., Sauvage, B., Nédélec, P., Blot, R. and Fan, S.: Global
695 tropospheric ozone trends, attributions, and radiative impacts in 1995–2017: An integrated
696 analysis using aircraft (IAGOS) observations, ozonesonde, and multi-decadal chemical

697 model simulations, *Atmospheric Chemistry and Physics*, 22(20), 13753–13782,
698 doi:10.5194/acp-22-13753-2022, 2022.

699 Wang, M. and Fu, Q.: Stratosphere-troposphere exchange of Air Masses and ozone
700 concentrations based on reanalyses and observations, *Journal of Geophysical Research:*
701 *Atmospheres*, 126(18), doi:10.1029/2021jd035159, 2021.

702 Waugh, D. W. and Polvani, L. M.: Climatology of intrusions into the tropical upper troposphere,
703 *Geophysical Research Letters*, 27(23), 3857–3860, doi:10.1029/2000gl012250, 2000.

704 White, I. P., Lu, H., and Mitchell, N. J.: Seasonal evolution of the QBO-induced wave forcing
705 and circulation anomalies in the northern winter stratosphere, *Journal of Geophysical*
706 *Research: Atmospheres*, 121, 10,411–10,431, <https://doi.org/10.1002/2015jd024507>, 2016.

707 Williams, R. S., Hegglin, M. I., Jöckel, P., Garny, H. and Shine, K. P.: Air quality and radiative
708 impacts of downward-propagating sudden stratospheric warmings (ssws), *Atmospheric*
709 *Chemistry and Physics*, 24(2), 1389–1413, doi:10.5194/acp-24-1389-2024, 2024.

710 Williams, R. S., Hegglin, M. I., Kerridge, B. J., Jöckel, P., Latter, B. G. and Plummer, D. A.:
711 Characterising the seasonal and geographical variability in tropospheric ozone, stratospheric
712 influence and recent changes, *Atmospheric Chemistry and Physics*, 19(6), 3589–3620,
713 doi:10.5194/acp-19-3589-2019, 2019.

714 Xia, Y., Xie, F. and Lu, X.: Enhancement of Arctic surface ozone during the 2020–2021 winter
715 associated with the sudden stratospheric warming, *Environmental Research Letters*, 18(2),
716 024003, doi:10.1088/1748-9326/acaee0, 2023.

717 Zhang, J., Zhang, C., Zhang, K., Xu, M., Duan, J., Chipperfield, M. P., Feng, W., Zhao, S., and
718 Xie, F.: The role of chemical processes in the quasi-biennial oscillation (QBO) signal in
719 stratospheric ozone, *Atmospheric Environment*, 244, 117906,
720 <https://doi.org/10.1016/j.atmosenv.2020.117906>, 2020.

721 Ziemke, J. R., Chandra, S. and Bhartia, P. K.: “cloud slicing”: A new technique to derive upper
722 tropospheric ozone from satellite measurements, *Journal of Geophysical Research:*
723 *Atmospheres*, 106(D9), 9853–9867, doi:10.1029/2000jd900768, 2001.

724